OAK RIDGE NATIONAL LABORATORY

MANAGED BY UT-BATTELLE FOR THE DEPARTMENT OF ENERGY

Dr. Jeremy T. Busby
Materials Science and Technology Division
P.O. Box 2008 – MS-6138
Oak Ridge, TN 37831-6138
Telephone: (865) 241-4622
Fax: (865) 241-3650
E-mail: busbyjt@ornl.gov

ORNL//TM-2009/121

September 29, 2009

R. Reister
NE-31/Germantown Building
U.S. Department of Energy
1000 Independence Ave., S.W.
Washington, DC 20585-1290

Subject: Completion of LWRSP Level 2 Milestone (M2LOR10MAT13012), Report on FY09 testing and analysis of reactor metal degradation, due 9/30/2009

Dear Sir;

The objective of this letter is to inform you of progress on testing in the Reactor Metals Work Package within the Materials Aging and Degradation Pathway. As you know, structural components for nuclear reactors must tolerate high temperatures, a water environment, stress, vibration, and an intense neutron field. Degradation of materials in this environment can be life limiting and result in costly repairs, replacements, and loss of operating time, which can have significant effects on the commercial viability of a plant. A key step in assessing the viability of extended operation is evaluating the response of materials to greater neutron fluences, greater exposure to a corrosive environment, and/or, greater exposure to stress.

The strategic objectives of the Nuclear Materials Aging and Degradation R&D pathway are to develop the scientific basis for understanding and predicting long-term environmental degradation behavior of materials in nuclear power plants and to provide data and methods to assess performance of SSCs essential to safe and sustained nuclear power plant operations. Research is expected to lead to improved mechanistic understanding of key degradation modes as well as sufficient experimental data to provide and validate operational limits. Mechanistic and operational data will also be used to develop performance models for key material systems and components in later years.

To support this vision, three research tasks have been initiated in FY 2009 to examine degradation of reactor metals. These include High Fluence Effects on Reactor Pressure Vessel Steels, Mechanisms of Irradiation-Assisted Stress Corrosion Cracking, and Crack Initiation in Ni-base Alloys. As we reported in April, work was initiated in all three areas and the first data has been produced.

The objectives of each effort are described below. While reduced funding levels limited the Ni-base alloy crack initiation task to primarily planning activities, more significant accomplishments were made in the RPV and IASCC tasks. Those achievements for the RPV and IASCC tasks are attached to this letter.

Embrittlement of Reactor Pressure Vessel Steels: Extending operation to 80y will result in a doubling of the neutron exposure and increased operating power level will further increase the fluence to RPV steels. This task provides an evaluation of pressure vessel steels at high fluences for embrittlement and/or late blooming phases. A series of previously irradiated specimens of various materials, both model alloys and commercial steels for application in light-water reactor pressure vessels (RPV) and in the fusion reactor, were removed from an ORNL

hot cell storage facility. These specimens were irradiated in the BR-2 research reactor at SCK-CEN in Mol, Belgium at neutron fluxes from $3x10^{12}$ to $1x10^{14}$ n/cm^2 (>1 MeV) at 300°C and to fluences from $1.6x10^{19}$ to $1.3x10^{20}$ n/cm^2 (>1 MeV). The specimens were designed for microhardness and various microstructural examinations such as small-angle neutron scattering (SANS) and atom probe tomography (APT) provide an early opportunity for initial evaluations.

Mechanisms of Irradiation-Assisted Stress Corrosion Cracking: IASCC is currently a problem in LWR components and will become more severe and affect more materials, components, systems, and subsystems with increasing fluence and lifetime. Unfortunately, the mechanisms of IASCC are poorly understood, despite several decades of applied research. This task will utilize specimens previously irradiated as part of a past international research effort. These samples provide an opportunity for single-variable experiments to help identify mechanisms of IASCC. This effort has been initiated in FY09 and involves a partnership with EPRI. EPRI and DOE are both contributing one-half the total cost of this anticipated 5-year effort. Complementary efforts originally proposed at PNNL and ORNL have been deferred to FY10 due to the reduced funding available.

Crack Initiation of Nickel Base Alloys: Cracking of Ni-base alloys used in steam generator and piping components is currently a concern in LWR operations. This mode of degradation is expected to grow more severe with extended service time due to added stress and exposure to the reactor coolant. This research task provides an evaluation of surface effects and precursor states on crack initiation of Ni-base alloys. Crack growth rate tests and microstructural analysis will help provide a more mechanistic understanding of crack initiation and growth processes. This project will address one of the most critical unknowns for failure in light-water reactor (LWR) structural alloys: stress-corrosion crack initiation. Research will investigate important material (composition, processing and microstructure) and environmental (water chemistry, temperature and electrochemical potential) effects on the susceptibility to intergranular stress corrosion cracking (IGSCC) of corrosion-resistant nickel-base alloys. The focus of the work will be to identify mechanisms controlling IGSCC nucleation under realistic LWR conditions. Results will establish the framework to effectively model and mitigate crack initiation processes. Initial planning has resulted in a mature test frame design and sample matrix.

In summary, work has been initiated in all three reactor metal tasks. I'm very pleased with the amount and quality of work performed in this initial year. The collaborations and contributions to date are a significant first step in helping assure safe and efficient operation of the current LWR fleet during extended service.

If you have any comments or questions, please contact me. Thank you.

Sincerely,

Dr. Jeremy T. Busby
Senior Research Scientist
Materials Science and Technology Division
Oak Ridge National Laboratory

CC: R. Szilard, INL
S. Greene, ORNL
D. Ingersoll, ORNL
R. Nanstad, ORNL
G.R. Odette, University of California-Santa Barbara
G. Was, University of Michigan

Annual Progress Report

September 26, 2009

High-Fluence Effects on RPV Steels

G. Robert Odette

University of California, Santa Barbara

Randy K. Nanstad

Oak Ridge National Laboratory

I. INTRODUCTION

Current regulations require RPV steels to maintain conservative margins of fracture toughness so that postulated flaws do not threaten the integrity of the RPV during either normal operation and maintenance cycles or under accident transients, like pressurized thermal shock. Neutron irradiation degrades fracture toughness, in some cases severely. Thermal aging, while not generally considered a significant issue for a 40-y operating life, must be an additional consideration for operation to 60 or 80 years. Regulations, codified in the ASME Boiler and Pressure Vessel Code, Regulatory Guide 1.99 Rev 2, etc., recognize that embrittlement has a potential for reducing toughness below acceptable levels.

The last few decades have seen remarkable progress in developing a mechanistic understanding of irradiation embrittlement. This understanding has been exploited in formulating robust, physically-based and statistically-calibrated models of CVN-indexed transition-temperature shifts (TTS). These semi-empirical models account for key embrittlement variables and variable interactions, including the effects of copper (Cu), nickel (Ni), phosphorous (P), fluence (ϕt), flux (ϕ), and irradiation temperature (T_i). However, these models and our present understanding of radiation damage are not fully quantitative, and do not treat all potentially significant variables and issues.

Over the past three decades, developments in fracture mechanics have led to a number of consensus standards and codes for determining the fracture toughness parameters needed for development of databases that are useful for statistical analysis and establishment of uncertainties. The CVN toughness, however, is a qualitative measure, which must be correlated with the fracture toughness and crack-arrest toughness properties, K_{Ic} and K_{Ia}, necessary for structural integrity evaluations. Where practicable, direct measurements of the fracture toughness properties are desirable to reduce the uncertainties associated with correlations. Moreover, fracture-toughness data have been obtained in sufficient quantity to permit probabilistic application.

The progress notwithstanding, however, there are still significant technical issues that need to be addressed to reduce the uncertainties in regulatory application. The major issues regarding irradiation effects are summarized in [1,2]. Of the many significant issues discussed, those deemed to have the most impact on the current regulatory process are: (1) high fluence, long irradiation times, and flux effects, (2) material variability and surrogate materials, (3) high-nickel materials, (4) the fracture toughness master curve, (5) the bias in reference toughness derived from precracked Charpy specimens, (6) attenuation, (7) modeling and microstructural analysis, (8) thermal annealing and reirradiation, and (9) thermal aging. Material variability and surrogate materials are an overarching issue. A more complete understanding of the other issues is needed in

order to reduce the uncertainties associated with material variability. Moreover, the combination of irradiation experiments with modeling and microstructural studies provides an essential element in aging evaluations of RPVs.

It is clear that embrittlement of RPV steels is a critical issue that may limit LWR plant life extension. The primary objective of the LWRSP RPV task is to develop robust predictions of transition temperature shifts (TTS) at high fluence (ϕt) to at least 1020 n/cm2 (>1 MeV) pertinent to plant operation for 80 full power years. New and existing databases will be combined to support developing physically based models of TTS for high fluence-low flux (ϕ < 10 11/n/cm2-s) conditions, beyond the existing surveillance database.

A summary of progress on the RPV task of the LWRSP Materials Pathway is presented here.

II. IRRADIATION AND LOW TEMPERATURE ANNEALING RESPONSE

We have previously shown that short time (t), low temperature (T), a very light post irradiation anneal (PIA) at 350°C/5h recovers the unstable matrix defects (UMD) contribution, but leaves the stable matrix features (SMF) and copper-rich precipitates (CRP) contributions largely unaffected. Based on these studies we developed a three-feature TTS model that accounts for these complex and counterintuitive effects. However, this model was based on a very limited low fluence data. Thus, our current effort is to refine and validate the three-feature model based on a large matrix of alloys irradiated at a range of fluxes spanning more than three orders of magnitude up to fluences in excess of 10^{20} n/cm^2 at the highest flux. PIA is being performed in conjunction with microstructural studies, including small angle neutron scattering (SANS) and atom probe tomography (APT) to quantify the flux-dependent UMD, SMD and CRP contributions. The high flux irradiations were carried out in the BR2 reactor at ≈ 10^{14} n/cm^2-s at 4 fluences up to $1.3\text{x}10^{20}$ n/cm^2 and at an intermediate flux of ≈ $2\text{x}10^{12}$ n/cm^2-s to $2.1\text{x}10^{19}$ n/cm^2. The lower flux irradiations were carried out in the IVAR facility from ≈ 0.8 to $10\text{x}10^{11}$ n/cm^2/s in ranges of overlapping fluence up to $3.6\text{x}10^{29}$ n/cm^2. A large number of RPV steels and several simple model alloys were included in the BR2 irradiation in the form of two 0.5x3x26 mm coupons per material. While, the amount of irradiated material is limited it provides an adequate basis for extensive microstructural and hardness post irradiation annealing experiments.

As illustrated in Figure 1, the preliminary results of these studies are very encouraging. Irradiation-induced microhardness changes for a Cu-free pressure vessel steel irradiated over a range of flux and fluence are shown. The diamond, circle, and square symbols are for high (H), intermediate (I) and low (L) flux, respectively, with filled and open symbols for the irradiated and annealed conditions, respectively. The solid line represents the trend that is observed in low flux test reactor (IVAR) and surveillance (PREDB) irradiations. As predicted by the three-feature model, PIA results in large recovery of hardness for the high flux irradiations (red data points), presumably by removing the UMD leaving only the SMF contribution. The PIA high flux data fall below the surveillance predictions consistent with the predicted delay in the SMF hardening for this Cu-free material. Corresponding delays in CRP hardening in Cu bearing alloys have been confirmed in recent SANS studies. As expected, the high flux hardness also recovers more than that for the lower flux irradiations.

As shown by the hardness data in Figure 1, high flux irradiations produce significantly greater hardening at high fluences than do low flux irradiations (compare the I-H data with the IVAR/PREDB trend curve). These very preliminary results support the conclusion that blind use of high flux data for TTS predictions could be very misleading and hugely detrimental to extended vessel life. More generally, however, they represent only a small fraction of insight and information that can be gained from systematic science-based approaches to building mechanism-based TTS models.

Further PIA experiments have been performed at 350°C-5h with four alloys to anneal UMDs. Figure 2 shows an example for HSSI Weld 73W, a submerged-arc weld with 0.31 wt% copper and 0.60-wt% nickel. The PIA treatment to remove UMD (open triangles) shows that the high flux BR2 irradiation delays SMF and CRP contributions (as expected) leading to overprediction (rather than underprediction) of the hardening without UMD except at the highest fluence where CRP contributions saturate and a new late-blooming phase (LBP) contribution may begin.

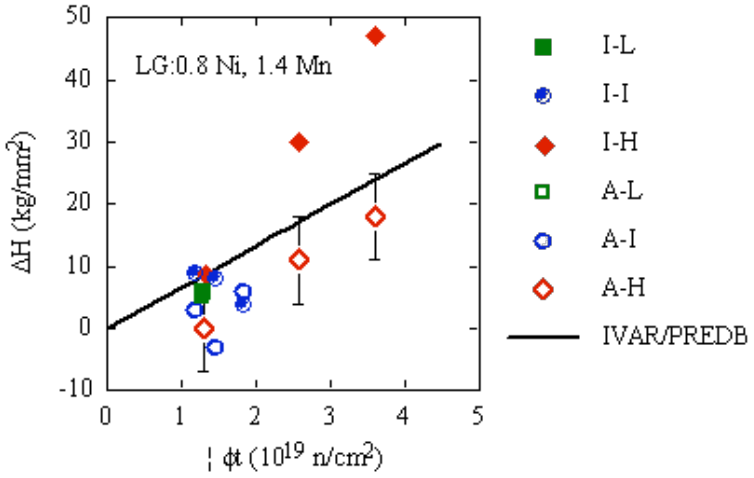

Figure 1 Microhardness changes vs the square root of neutron fluence (>1 MeV) for a Cu-free pressure vessel steel irradiated (I) and post-irradiation annealed (A) over a range of flux and fluence. The diamond, circle, and square symbols are for high (H), intermediate (I) and low (L) flux, respectively, with filled and open symbols for the irradiated and annealed conditions, respectively. The solid line represents the trend that is observed in low flux test reactor (IVAR) and surveillance (PREDB) irradiations.

More generally, the differences between the IVAR/PREDB prediction and the experimental data indicate a new mechanism is at work. More data are required to fully evaluate these effects.

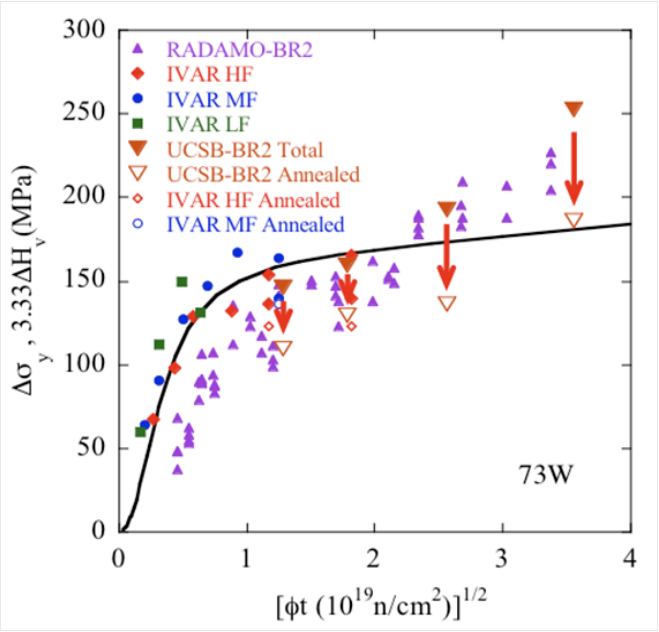

Figure 2. The PIA treatment for Weld 73W to remove UMDs (open triangles) shows that the high flux BR2 irradiation delays SMF and CRP contributions (as expected) leading to overprediction (rather than underprediction) of the hardening without UMD except at the highest fluence where CRP contributions saturate and a new late-blooming phase (LBP) contribution may begin.

Small-angle neutron scattering (SANS) experiments have also been performed by UCSB with five model alloys, one commercial model alloy, and a commercial weld, HSSI Weld 73W. Figures 3 (a)-(d) shows the results for Weld 73W.

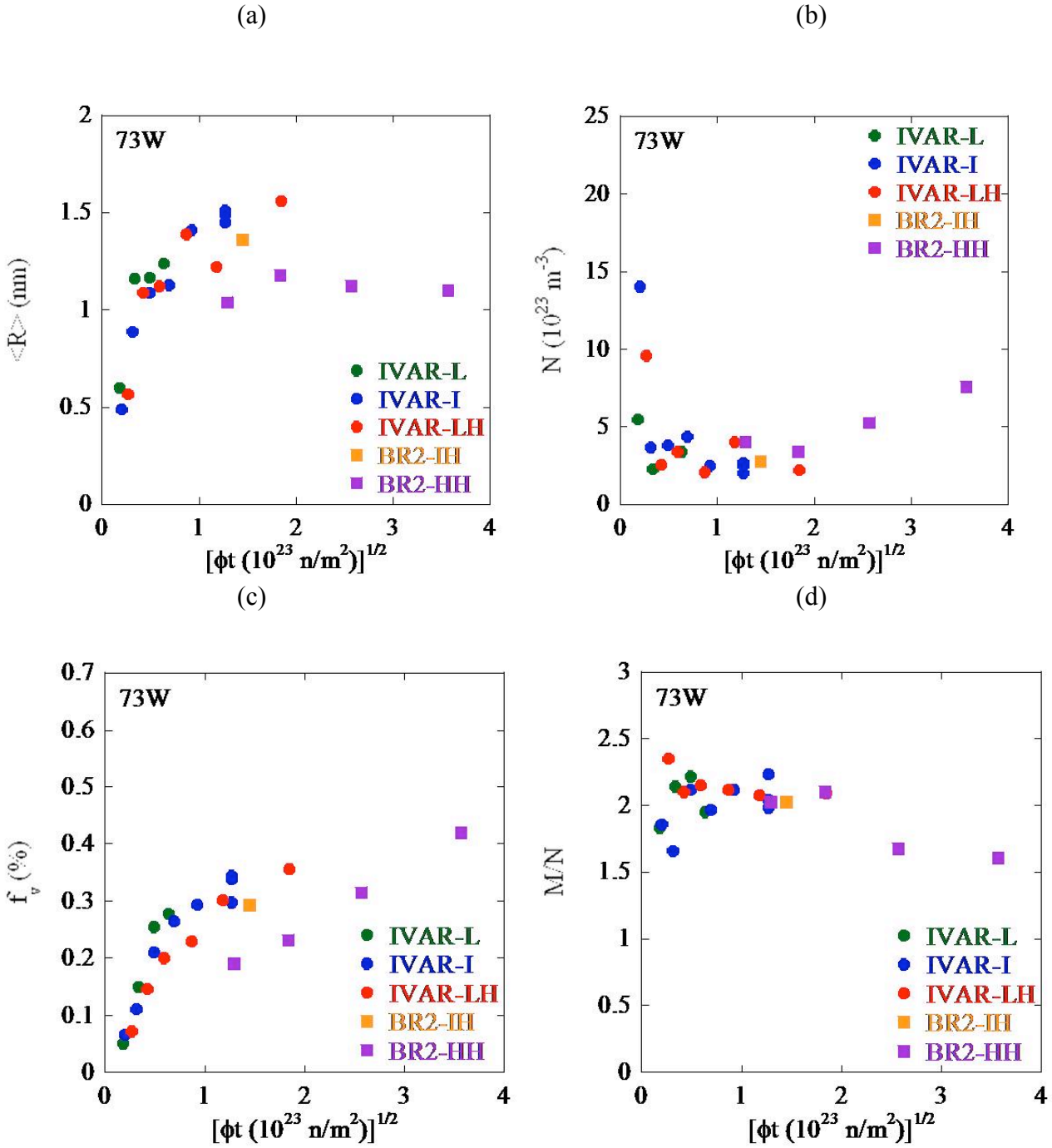

Figure 3. Results of small-angle scattering experiments for HSSI Weld 73W showing CRP (a) radius, (b) number density, (c) volume fraction, and (d) magnetic/nuclear scattering ratio vs square root fluence, and for IVAR irradiations at low flux and BR2 irradiations at high flux.

The results of these SANS experiments for Weld 73W show that at low fluence the CRPs that form at high flux are generally similar to this that evolve at lower flux. However, in the former case the CRPs are smaller (r) and only slightly more numerous (N) at low fluence. Thus at high flux, higher fluences are needed to produce the same volume fraction (f) of precipitates. In addition to this anticipated delay in CRP evolution, the high flux irradiations result in an increase in the N with increasing fluence in contrast to a decreasing N that is generally observed at low fluence. A decrease in the magnetic to nuclear scattering ratio (M/N) is also observed at high flux and fluence, consistent with emergence of precipitates with higher Mn and Ni contents, characteristic of LBP.

Motivated by the LWRSP RPV task, UCSB submitted a proposal that was accepted by the National Science User Facility Advanced Test Reactor Irradiation Facility. That facility will be utilized for an irradiation project at a intermediate high flux ($4.5x10^{12}$ n/cm^2-s) to a high fluence ($\approx 10^{20}$ n/cm^2) and will take about one year to complete the irradiation campaign. This experiment will begin to answer the need for a new high fluence, intermediate flux dataset to couple to a large body of existing data for a large set of common alloys (≥ 100) irradiated over a wide range of flux and fluence. The Small I position of the ATR NSUF will be used for the capsules with a thermal neutron shield and active temperature control. More than 2000 specimens, including disc compact tension, disc multipurpose coupons, mini-tensile, etc. will be included in the experiment.

III. SUMMARY

In summary, the RPV task has obtained initial data demonstrating differences between low flux IVAR prediction and high flux BR2 data that demonstrate a significant dose rate effect, likely involving a new mechanism. More data are required to fully evaluate these effects, but thermal annealing studies are showing the significance of unstable matrix defects, as defined by recovery at low annealing temperatures and short times, in high flux irradiations and the potential for a three-feature model of irradiation embrittlement incorporating UMDs. FY10 activities will include initiation of irradiations in the ATR at INL, and development of detailed plans for further irradiations, thermal annealing studies, and studies to resolve the other identified RPV issues.

Semi-Annual Progress Report
August 31, 2009

Identifying Mechanisms and Mitigation Strategies for Irradiation Assisted Stress Corrosion Cracking of Austenitic Steels in LWR Core Components

Gary S Was
Yugo Ashida
University of Michigan

During the project start-up period from April through July 2009, we performed test system construction, gathered information on samples tested in other institutions, and conducted preliminary CGR tests. Two CGR tests were completed on solution annealed 316L stainless steel in air at room temperature. The functionality of reversed DCPD technique and the accuracy in monitoring crack growth length were confirmed. The results suggest that the percentage error of DCPD estimation is about 0.5% for fatigue crack propagation in air. The loading system and DCPD monitoring system were stable over several hundred of hours of testing. This test system is ready for CGR tests in high temperature water.

1. Fabrication of Autoclave System IM3 for CGR Testing

Figure 1 shows the testing systems and the layout in the Irradiated Materials Testing Laboratory (IMTL) at the University of Michigan. High temperature water testing systems IM1 and IM2 are dedicated for CERT and CGR tests, respectively. Another system IM3 for CGR testing is under construction and will be finished in September 2009. Each of these autoclaves can be moved into hot cell #1 for the loading of neutron-irradiated samples. A SEM system is also available for sample analysis in the hot cell. IM4 and IM5 are our future systems.

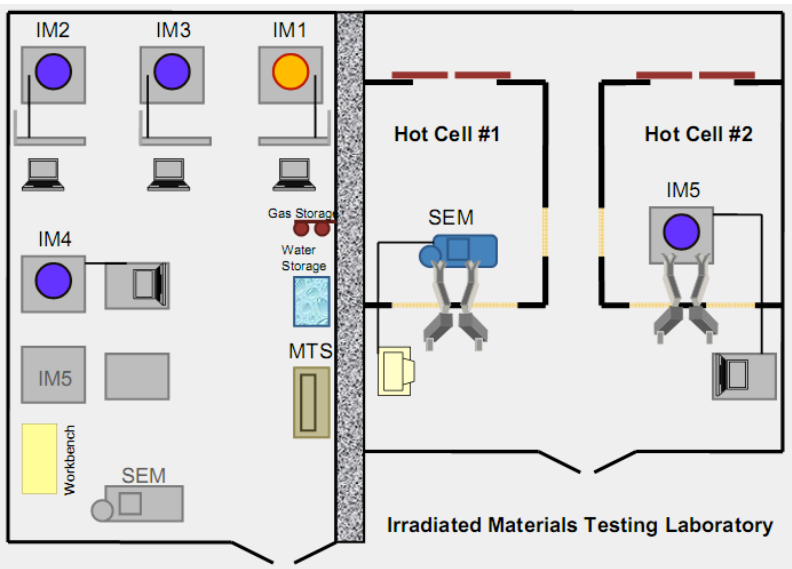

Figure 1. Testing systems in Irradiated Materials Testing Laboratory.

Figure 2 shows the autoclave installation. Each testing system consists of a 4 L autoclave, low and high temperature water loop and flow control system, water chemistry monitoring system, loading system, and data

collecting system. Each system is also equipped with a reversed DCPD monitoring system. The CERT system can test four tensile samples simultaneously. All irradiated samples in this program will be shielded and tested in IMTL.

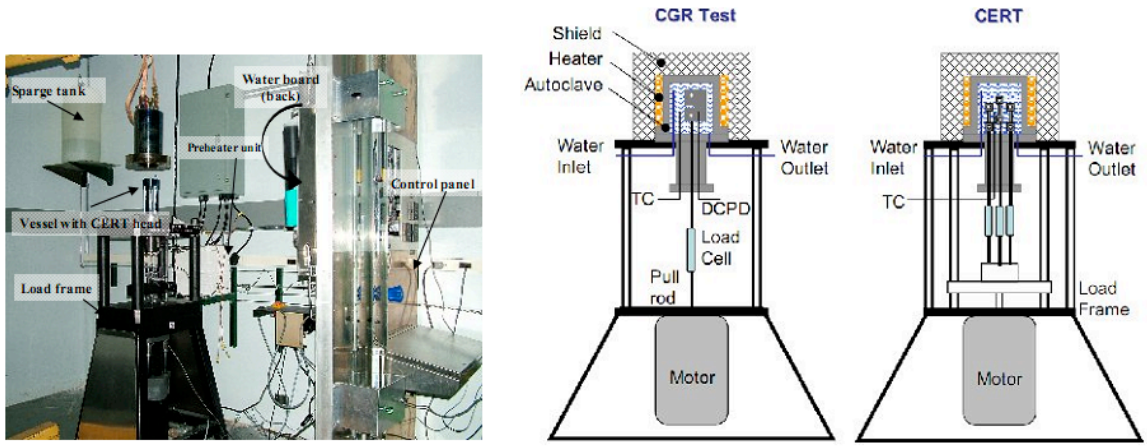

Figure 2. Autoclave system and setup for CGR and CERT testing.

2. Procurement of Neutron-Irradiated Samples and Data Gathering on Previously Tested Samples

Neutron-irradiated samples consisting of 6 RCT specimens and 32 tensile specimens will be shipped from Studsvik to ORNL, and then to the University of Michigan. Table 1 provides the RCT sample inventory and Table 2 provides the sample inventory for tensile samples.

Table 1. RCT inventory for this program.

Specimen No.	BS01	GS01	IP01	MS01	NS01	PS02
Heat Serial	BS	GS	IP	MS	NS	PS
Material	316	304	304 (SA 304L)	304	304	316L
Material Type	SA, Baffle Bolt	HP	HP	HP	HP	HP
Solute Additions	None	Mo	- C, P	Ti	Nb	Hf
Dose, dpa	5.5	11.8	4.4	10.7	10.7	9.6
Reactor	Boris 6	Boris 6	Boris 7	Boris 7	Boris 7	Boris 7
Date of Out the Reactor	Oct. 2001	Oct. 2002	June, 2004	June, 2004	June, 2004	Oct. 2003
Specimen Type	RCT	RCT	RCT	RCT	RCT	RCT
Specimen Thickness	8mm?	6mm?	6mm?	6mm?	6mm?	6mm?

In this quarter, we also contacted other institutions conducting CGR tests on RCTs in the CIR program. Studsvik, SCK-CEN and NRI all kindly provided us with information on their CGR tests. The information includes specimen type and dimensions, dose, radioactivity, test conditions such as loading and water chemistry, and some of the published test results. A literature review on CIR reports and other IASCC related publications is also an essential part of this project that is underway.

Table 2. Tensile specimen inventory for this program.

No.	Specimen	Material	Material Type	Heat Serial	Solute Additions	Reactor	Date out of reactor	Dose, dpa
1	AS13	304L	SA, Shroud	AS	None	Boris 6	Oct., 2001	5.5
2	AS14	304L	SA, Shroud	AS	None	Boris 6	Oct., 2001	5.5
3	AS17	304L	SA, Shroud	AS	None	Boris 6	Oct., 2002	10.2
4	AS18	304L	SA, Shroud	AS	None	Boris 6	Oct., 2002	10.2
5	AS19	304L	SA, Shroud	AS	None	Boris 6	Oct., 2002	10.2
6	BS13	316	SA, Bolt	BS	None	Boris 6	Oct., 2001	5.5
7	BS16	316	SA, Bolt	BS	None	Boris 6	Oct., 2002	10.2
8	BR15	316	CW, Bolt	BR	None	Boris 6	Mar., 2003	4.8
9	B124(2)	316	CW, Bolt	B	None	Boris 6	Mar., 2003	25
10	B125(3)	316	CW, Bolt	B	None	Boris 6	Mar., 2003	25
11	B126	316	CW, Bolt	B	None	Boris 6	Mar., 2003	25
12	CR13	316	CW, Ti St.	CR	Ti	Boris 6	Mar., 2003	4.8
13	CR14	316	CW, Ti St.	CR	Ti	Boris 6	Mar., 2003	4.8
14	(CR17)	316	CW, Ti St.	CR	Ti	Boris 6	Mar., 2003	25
15	(CR18)	316	CW, Ti St.	CR	Ti	Boris 6	Mar., 2003	25
16	CR19	316	CW, Ti St.	CR	Ti	Boris 6	Mar., 2003	25
17	ES13	304	HP	ES	None	Boris 6	Oct., 2002	11.8
18	ES14	304	HP	ES	None	Boris 6	Oct., 2002	11.8
19	ES16	304	HP	ES	None	Boris 6	Oct., 2002	10.2
20	GS13	304	HP	GS	Mo	Boris 6	Oct., 2002	11.8
21	GS14	304	HP	GS	Mo	Boris 6	Oct., 2002	11.8
22	AS22	304L	SA, Shroud	AS	None	Boris 7	June, 2004	47.5
23	AS23	304L	SA, Shroud	AS	None	Boris 7	June, 2004	47.5
24	BS18	316	SA, Bolt	BS	None	Boris 7	June, 2004	47.5
25	ES21	304	HP	ES	None	Boris 7	June, 2004	10.7
26	LS13	304	HP	LS	Cr, Ni	Boris 7	Oct., 2003	9.1
27	FS13	304	HP	FS	- C	Boris 7	Oct., 2003	9.1
28	HS13	304	HP	HS	Si	Boris 7	Oct., 2003	7.8
29	KS13	304	HP	KS	Ni	Boris 7	Oct., 2003	9.6
30	PS13	304	HP	PS	Hf	Boris 7	Oct., 2003	9.6
31	PS14	304	HP	PS	Hf	Boris 7	Oct., 2003	9.6
32	PS15	304	HP	PS	Hf	Boris 7	Oct., 2003	9.6
33	SW36	304L	SA, Swedish	SW	None	Boris 7	June, 2004	4.4
34	SW37	304L	SA, Swedish	SW	None	Boris 7	June, 2004	4.4

* CR17 and CR18 are missing; B122 and B123 are available.

3. Crack Growth Tests in Air and the Accuracy of Crack Length Estimation by DCPD

The purpose of this study is to continuously monitor the crack growth in a CT specimen by using reversed DCPD technique and to confirm the accuracy of DCPD estimated crack length. Two crack growth experiments were conducted on the same sample in air at room temperature.

Test material is solution annealed 316L stainless steel. The Specimen was 0.5T CT with 5% side groves introduced on each side of the specimen. As shown in Figure 3, the DCPD monitoring system consists of a DC power supply, relays, Nano-Volt meter, data acquisition unit, servomotor and Skala controller. A DOS program (At5), developed by Dr. Andresen at GE Global Research Center, was used to control current reversing (once per second) and the loading conditions (Kmax, R, and frequency), and to average and record DCPD data. The data processing program (HIKO) is based on DotNetFX2.0. As shown in Figure 4, a pair of current probes located along the centerline and 5 mm apart at the back edges of the specimen and a pair of potential probes at the two front corners were spot welded on the specimen. These probes were connected to the DCPD measuring system.

Two crack growth tests, T0526 and T0720, were conducted on the same sample. The crack was introduced from the notch of the CT specimen in T0526. Subsequent crack growth was continued on the same specimen in T0720. The current supply was 1.9 A for T0526 and 2.5 A for T0720. After test T0720, the fracture

surface was opened and the crack length increment in each loading step was measured and compared to that determined from the DCPD data.

Figure 5 shows beach marks on the fracture surface. The crack propagated evenly and the beach marks were observed because the crack propagation at R=0.7 shows a different appearance from those at R=0.3 and R=0.5. This also can be seen in Figure 6 (SEM photos). Tables 3 and 4 show the loading conditions and the crack growth results in T0526 and T0720, respectively. The CGR data for each loading step include a calculation of the estimated crack increment determined by dividing the DCPD result by loading time, a fitting result acquired from AT5 or HIKO program, and the measured crack length divided by loading time. Figure 7 shows the same result in Table 3, but for an additional 0.07 mm in crack length, because the initial potential shift during the constant loading period was not subtracted from the total potential. In Figure 8, the initial potential shift was reset after initiation of constant loading.

The percentage error in the DCPD estimation was calculated by the following:

%error = 100% * (DCPD estimation – Actual Crack Length) / Actual Crack Length (1)

The DCPD estimations are 0.957 mm for T0526 and 7.45 mm for T0720, and the actual measurements on the fracture surface are 1.200 mm for T0526 and 7.412 mm for T0720. Accordingly, the total percentage errors of DCPD are –20.3% for T0526 and 0.5% for T0720, respectively. It needs to be noted that the current supply of 1.9A in T0526 was 24% lower than that of 2.5A in T0720. The low current supply probably reduced crack length resolution because of getting more noise. The percentage error is roughly proportional to change in current.

As discussed, accurate CGR evaluation can be acquired for fatigue crack growth in air when the CGR was higher than $1x10^{-6}$ mm/s. However, potential drop resolution may be affected by the irregularly crack front at very low CGR. Other researchers [1-3] have reported crack length underestimation by DCPD in the case of SCC in high temperature water. Therefore, the accuracy of DCPD monitoring in simulated BWR environment needs to be examined in our next step experiment.

4. Preparations for Constant Extension Rate Tests (CERTs)

In this period, the preparation for CERTs focused on literature review, especially those test results generated on proton-irradiated samples. The test design on neutron-irradiated samples will benefit from the integration of information.

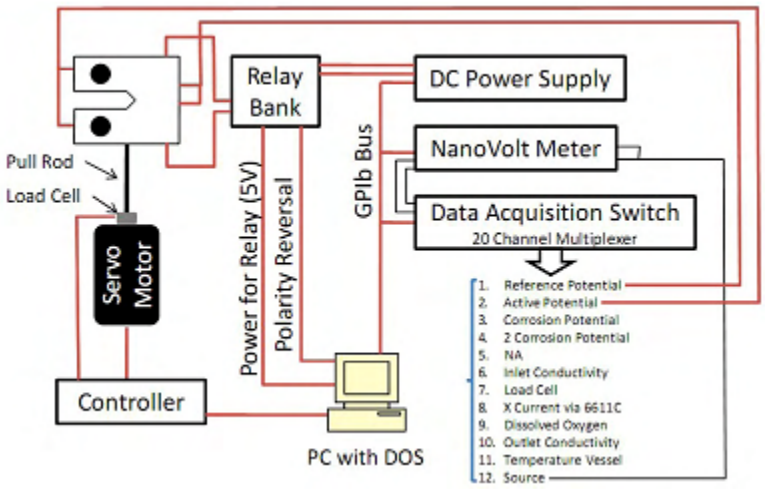

Figure 3. DCPD monitoring system.

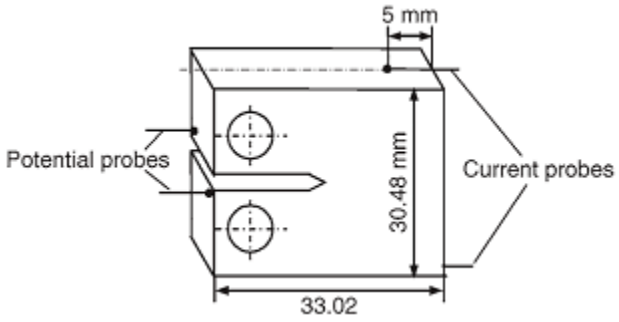

Figure 4. Arrangement of current and potential probes on the CT specimen.

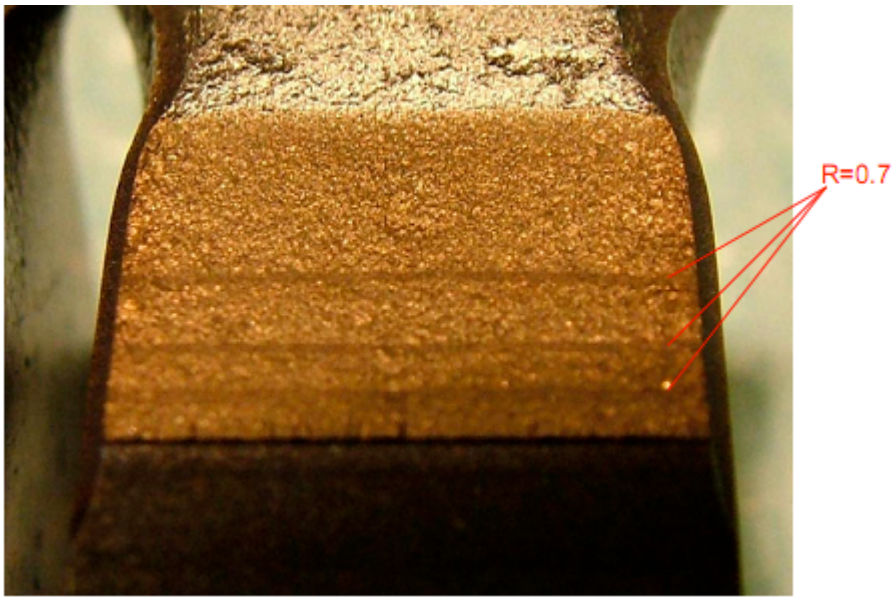

Figure 5. Beach marks on the fracture surface.

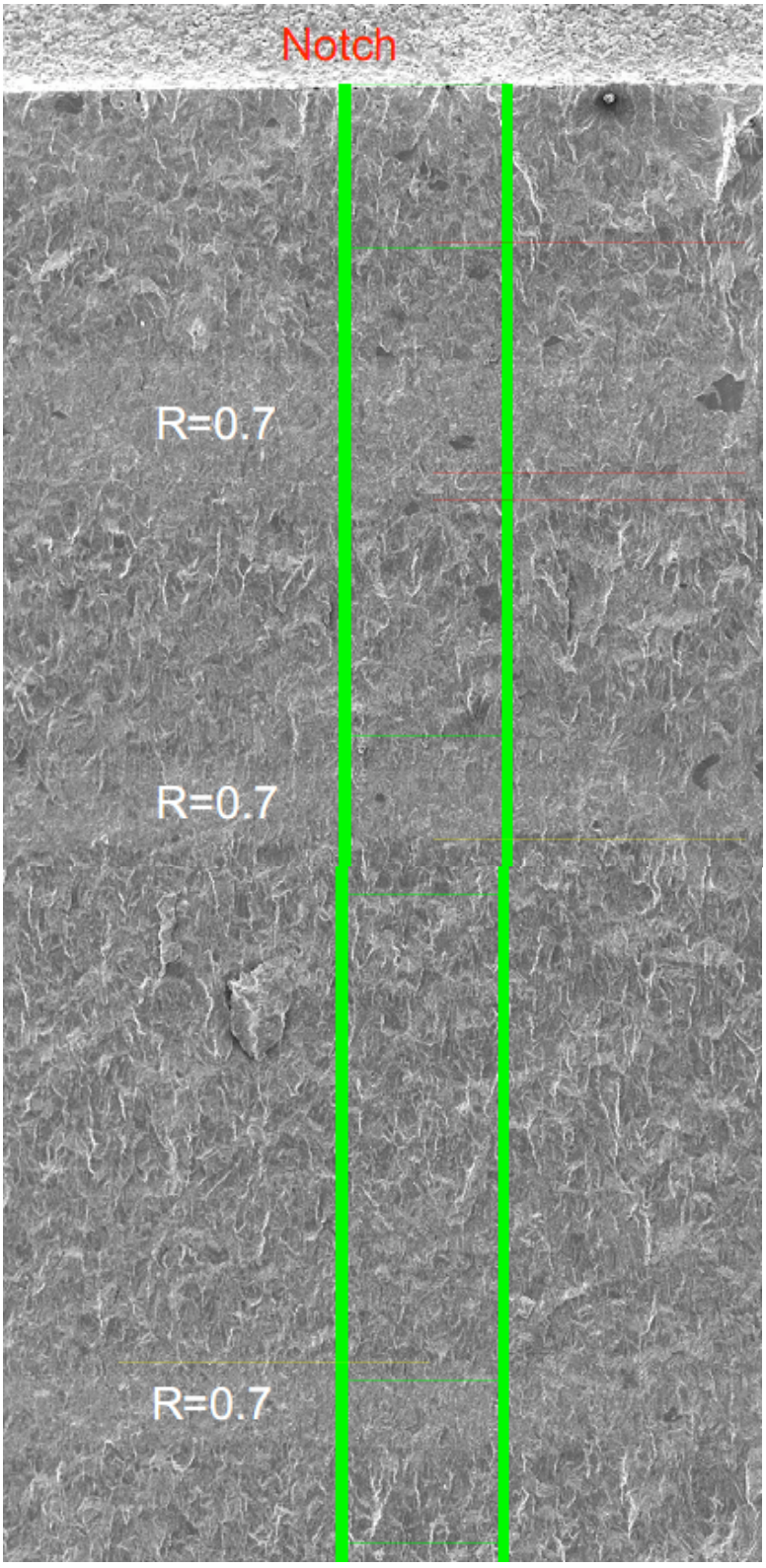

(a)

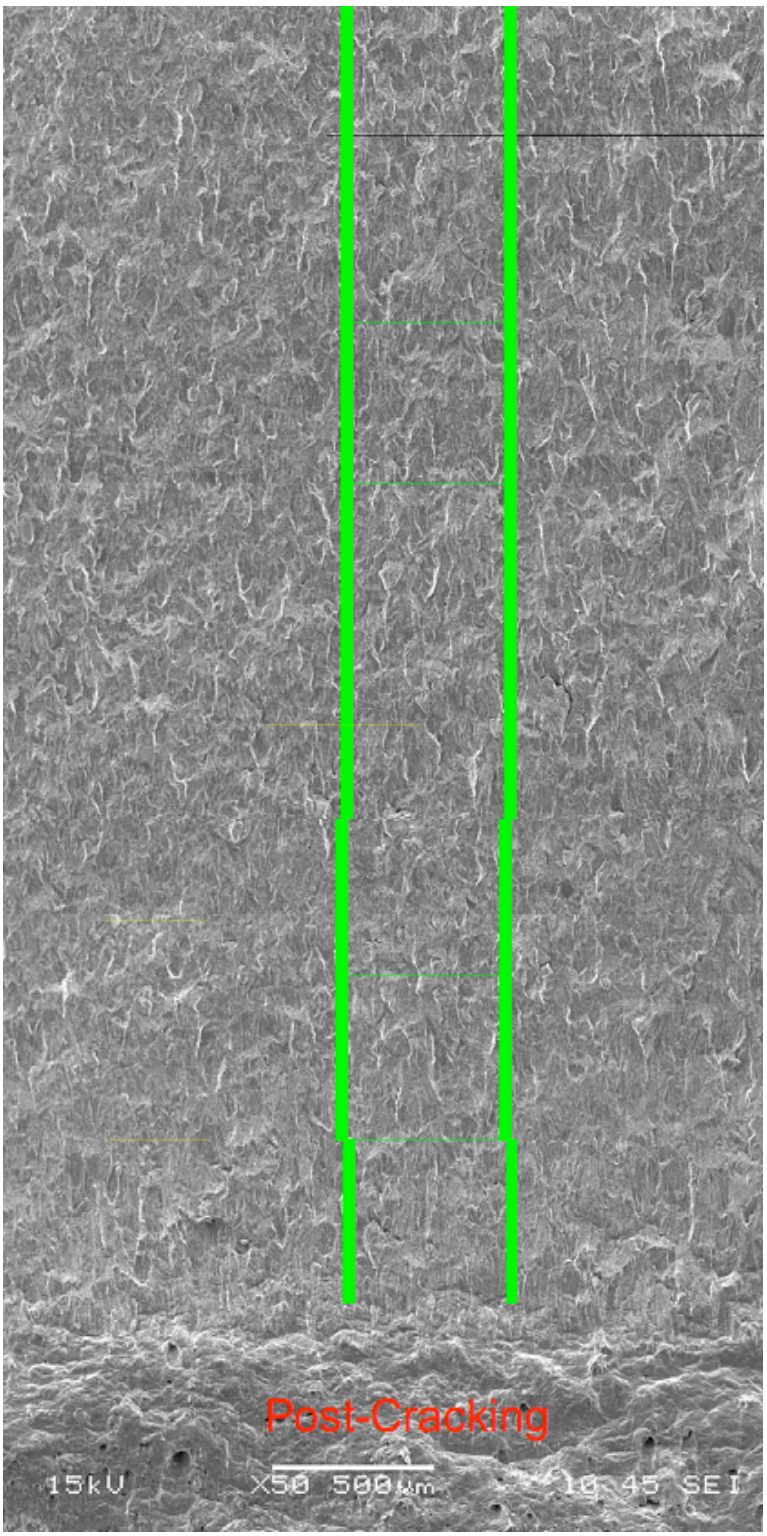

(b)

Figure 6. Morphology and actual crack length measurement (green strips) on the fracture surface showing different appearance at R=0.7. (a) Crack propagation from the notch; (b) Post-crack introduced after the CGR test.

Table 3. Loading conditions and crack growth results (T0526).

Step	Kmax ($MPa \cdot m^{1/2}$)	R (K_{min} / K_{max})	f (Hz)	Loading Mode	Loading Time (h)	Total Time (h)	Crack Increment (mm)	Total Crack Length (mm)	CGR* (mm/s)
1	0	-	-	-	0	25.5	0	0	0
2	30.25	1.0	-	Constant	5	30.5	0	0	0 (PD drift observed after loading)
3	30.25	0.3	0.5	Haversine	4	34.5	0.080	0.080	$5.56X10^{-6}$ ($6.02X10^{-6}$)
4	30.25	0.3	0.5	Haversine Auto. K	3.8	38.3	0.3 *0.486*	0.38 *0.486*	$2.19X10^{-5}$ ($2.17X10^{-5}$) *$1.73X10^{-5}$*
5	30.25	0.5	0.5	Haversine Auto. K	4.2	42.5	0.263 *0.337*	0.643 *0.823*	$1.74X10^{-5}$ ($1.50X10^{-5}$) *$2.23X10^{-5}$*
6	30.25	0.7	0.5	Haversine Auto. K	19.5	62.0	0.25 *0.377*	0.893 *1.200*	$3.56X10^{-6}$ ($3.36X10^{-6}$) *$5.37X10^{-6}$*
7	30.25	0.7	0.1	Haversine Auto. K	58	120.0	0.064 *0.377*	0.957 *1.200*	$3.07X10^{-7}$ ($6.20X10^{-7}$)
8	30.25	1.0	-	Constant Auto. K	22.5	142.5	0	0.957	0

* CGR: Crack Increment/Loading Time (at5 analysis) *Underline* : Actual Crack Growth on the Fracture Surface

Table 4. Loading conditions and crack growth results (T0720).

Step	Kmax ($MPa \cdot m^{1/2}$)	R (K_{min} / K_{max})	f (Hz)	Loading Mode	Loading Time (h)	Total Time (h)	Crack Increment (mm)	Total Crack Length (mm)	CGR* (mm/s)
0	30.25	1.0	-	Constant	1.5	1.5	0	0	0 (PD drift observed after loading)
1	30.25	0.3	0.5	Haversine Auto. K	1.7	3.2	0.24 *0.351*	0.24 *0.351*	$3.92X10^{-6}$ ($2.98X10^{-5}$) *$5.74X10^{-5}$*
2	30.25	0.5	0.5	Haversine Auto. K	8.1	11.3	0.556 *0.532*	0.796 *0.883*	$1.91X10^{-5}$ ($1.75X10^{-5}$) *$1.82X10^{-5}$*
3	30.25	0.7	0.5	Haversine Auto. K	19.2	30.5	0.204 *0.252*	1 *1.135*	$2.95X10^{-6}$ ($2.74X10^{-6}$) *$3.65X10^{-6}$*
4	30.25	0.3	0.5	Haversine Auto. K	8.2	38.7	1.03 *1.089*	2.03 *2.224*	$3.49X10^{-5}$ ($3.52X10^{-5}$) *$3.69X10^{-5}$*
5	30.25	0.5	0.5	Haversine Auto. K	10.5	49.2	0.52 *0.544*	2.55 *2.768*	$1.38X10^{-5}$ ($1.22X10^{-5}$) *$1.44X10^{-5}$*
6	30.25	0.7	0.5	Haversine Auto. K	16.9	66.1	0.23 *0.264*	2.78 *3.031*	$3.78X10^{-6}$ ($3.91X10^{-6}$) *$4.34X10^{-6}$*
7	30.25	0.7	0.1	Haversine Auto. K	24.5	90.6	0.07 *0.0*	2.85 *3.031*	$7.94X10^{-7}$ ($1.09X10^{-6}$) *0*
8	30.25	0.3	1	Haversine Auto. K	14.6	105.2	2.6 *2.540*	5.45 *5.571*	$4.95X10^{-5}$ ($4.73X10^{-5}$) *$4.83X10^{-5}$*
9	30.25	0.5	0.5	Haversine Auto. K	6.9	112.1	0.73 *0.599*	6.18 *6.170*	$2.94X10^{-5}$ ($2.79X10^{-5}$) *$2.41X10^{-5}$*
10	30.25	0.3	0.5	Haversine Auto. K	4	116.1	0.76 *0.671*	6.94 *6.841*	$5.28X10^{-5}$ ($5.04X10^{-5}$) *$4.66X10^{-5}$*
11	30.25	0.3	1	Constant Auto. K	5.7	121.8	0.51 *0.571*	7.45 *7.412*	$2.49X10^{-5}$ ($2.72X10^{-5}$)** *$2.78X10^{-5}$*

* CGR: Crack Increment/Loading Time (at5 analysis) ** Data recording had problem, re-calculated data *Underline* : Actual Crack Growth on the Fracture Surface

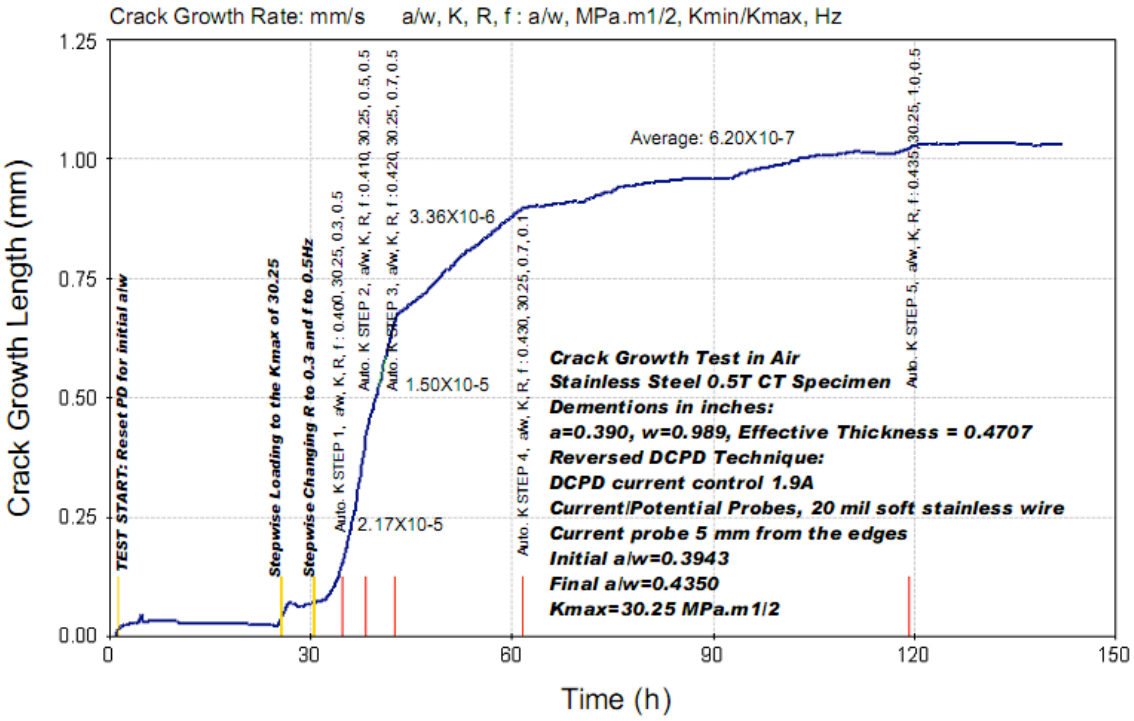

Figure 7. Crack length on 316L SS, 0.5T CT specimen in air (T0526) measured by DCPD. Estimated crack length is 0.957 mm with a correction of the initial potential shift. The low input current 1.9 A caused a percentage error of –20.3%.

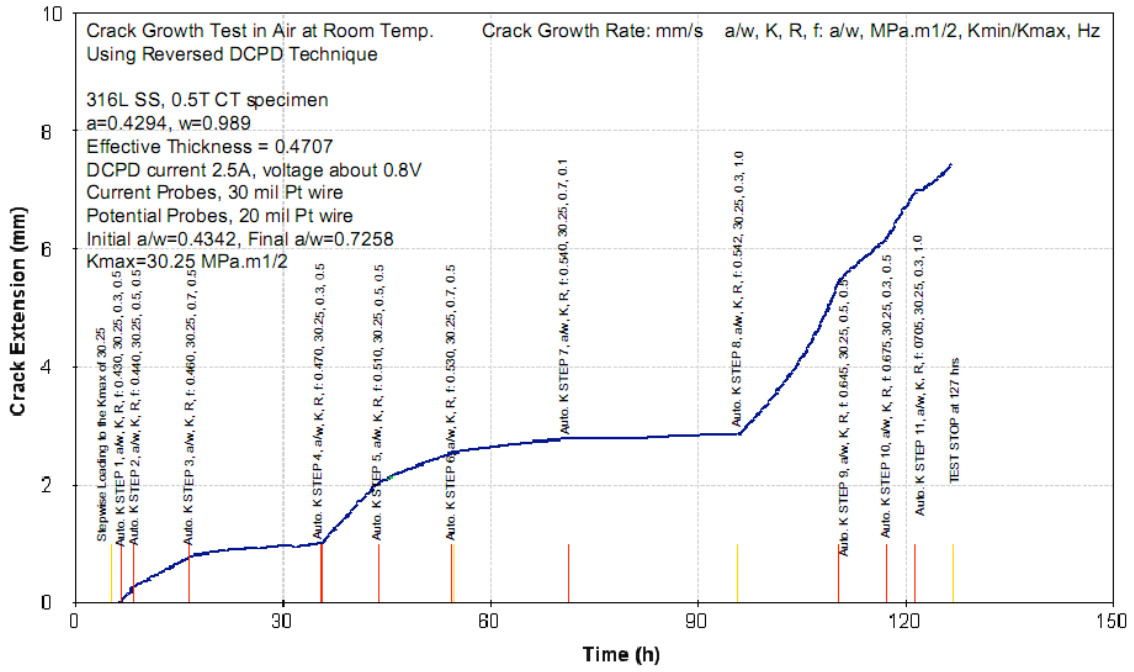

Figure 8. Crack length on 316L SS, 0.5T CT specimen in air (T0720) measured by DCPD. Estimated crack length is 7.45 mm and the total percentage error is 0.5%.

5. Project Milestones

Task#	*Task Description*	**Quarter** 4	5	6	7	8	9	10	11	12	1	2	3
1	**Build Autoclave System IM3 for CGR Testing**	-	-	-	-	-							
	Purchase Supplies and Parts	√	√										
	System Integration			√	√	⇒							
	Loading System			√									
	Electrical Supply				√	⇒							
	Water Loop				√	⇒							
	Crack Growth Monitoring System					⇒							
2	**Procure Neutron-Irradiated Samples**			-	-	-	-	-	-	-			
3	**Gather Information on Tested Samples**			-	-	-	-	-	-	-			
	Contact CIR institutions			√									
	Studsvik, SCK-CEN, NRI, ANL			√									
	Specimens, Dose, Radioactivity, Dimension, etc.			√									
	Test Conditions, Loading, Environment			√									
	Test Results, CGR, Microscopy, etc.			√	√	⇒			O	O			
4	**Crack Growth Tests**												
	Crack Growth in Air		√	√	√								
	DCPD functionality		√										
	Accuracy of DCPD monitoring CGR				√								
	Crack Growth in Simulated BWR Env.												
	0.5TCT specimen (20%CW, 316L)					⇒	O	O	O				
	0.4TCT specimen (20%CW, 316L)							O	O	O			
	Test Neutron-Irradiated RCT sample										O	O	O
5	**Constant Extension Rate Tests**												
	Literature Review on Proton Irradiated Samples				√	⇒							
	Decide Experimental combinations					⇒							
	Test Neutron-Irradiated Sample										O	O	O

√ Accomplished ⇒ Ongoing O Planed

REFERENCES

1. Q.J. Peng, S. Teysseyre, P.L. Andresen, and G.S. Was, "Stress Corrosion Crack Growth in Type 316 Stainless Steel in Supercritical Water", Corrosion, Vol.63 (2007) pp. 1033-1041.
2. W.J. Mills, "Stress Corrosion Cracking Response of 304 Stainless Steel in Aerated and Deaerated Water", Proc. 14th Int. Symp. On Environmental Degradation of Materials in Nuclear Power System-Water Reactor (T.R. Allen, ANS 2009).
3. Anders Jenssen, Johan Stjarnsater, Raj Pathania, "Crack Growth Rate Testing of Fast Reactor Irradiated Type 304L and 316 SS in BWR and PWR Environments", Proc. 14th Int. Symp. On Environmental Degradation of Materials in Nuclear Power System-Water Reactor (T.R. Allen, ANS 2009).